

## Response to the comments of Referee #1

We are grateful to the reviewer for his/her careful reading of the paper. The reviewer's comments helped us greatly to improve the presentation of our ideas and results. In what follows, we repeat each of the reviewer's comments in italic, and provide our response in roman.

*General Comments: This manuscript deals with one of the very important topics in EnKF data assimilation. The described localization functions for multiple state variables can be used both in EnKF and Variational Ensemble data assimilation systems. The schemes are extensively described and easy to follow. In addition, OSSE results with a low-dimensional system are presented to document benefit of the new schemes. I suggest accepting this paper after addressing the following comments.*

*Specific comments: 1. Is the localization function defined by Eqs. 8-9 a Gaussian-like function? As shown in Fig. 1, the plotted Askey function is not a Gaussian-like function, which might make it be problematic to filter a Gaussian-like error correlation pattern.*

The shape of the localization function does not affect the Gaussianity of the estimate of the distribution of the error, as it affects only second statistical moments. In other words, the estimate of the error distribution can still be Gaussian even if we use a localization function with a different shape, such as the Askey function.

*2. Need more details on experiment design, especially on experiment S3 and S4 (P847-848). For experiment S3, values of localization parameters should be described. For experiment S3 and S4, please also explain the rationales used to specify localization parameters.*

The values of the localization parameters  $\mu$  and  $\nu$  are given in the last paragraph of Section 3.c. We tried a few different values for each of these parameters and these values seem to work well. Results with various values for  $c$  and  $\beta$  are presented in Figs. 4-11.

*3. Sensitivity to number of ensemble members can be further studied. The presented results (Page 850) showed similar results when using 20- and 40-member ensembles. Is this because the use of localization schemes? The other question is that what is the critical number of ensemble member to produce a good multi-variable background error covariance (BEC) modeling for such a low-dimensional Lorenz-95 system? The BEC with very large*

*number of ensemble member could be used to valid which localization scheme is a better one. I suggest showing figures of the covariance in physical space to demonstrate the sensitivity with several number of ensemble members (e.g., 100, 200, 500, ...).*

We tried various ensemble sizes and we found that the state estimation error is not sensitive to the choice of ensemble size between 20 and 40. This may be due to the fact that we do localization, as the reviewer suggests.

Regarding the “critical number of ensemble members”, it is not our goal in this paper to find the optimal number of ensemble members. Rather, we compare various localization schemes given an ensemble size.

We now add experiments with 500-member ensemble in Figures 8-11. Please see our texts in Section 3.d for our description. The figures show that the localization scheme S4, which localizes the variance between  $X$  and  $Y$  and within each state variable, still performs better overall than the other localization schemes.

*Other minor comments: 1. Page 842, Eqs, 6-7, Please explain beta here.*

$\beta$  is a parameter, with magnitude less than 1, used to make the matrix  $\mathbf{C}$  positive definite (c.f.  $\mathbf{C}$  in (5)). We hope our explanation on that page is clear.

*2. Page 843, Eqs, 8-9, for real atmospheric data assimilation, do you have any ideas on rules to specify the related parameters in Eqs. 8-9?*

The parameters in Eqs. 8-9 should be determined by the characteristic of the state variables and their relationship. This obviously depends on the actual atmospheric data assimilation problem and the dynamic model.

*3. Page 836, Line 13, what are values of variances for the two state variables?*

We assume this comment is about page 846 (not page 836). The variances for  $X$ , variances for  $Y$ , and covariances between  $X$  and  $Y$  range from -4 to 4, -0.02 to 0.02, and -0.2 to 0.2, respectively.

*4. Page 847, Line 14, beta(i,j)=beta ?, please explain beta.*

$\beta$  here plays the same role as in Eqs. 6-7. We modified the sentence in line 14 to make it clear.

*5. Page 847, Line 21-22, Please speak more about the test results.*

We presented the test results including figures in Section 3.d in the revision.

*6. Page 850, Lines 14-16. Though I understand the statements are based on materials in Page 841, it seems to me the statement may confuse general readers. Actually, use of location functions is expected to alleviate the rank deficient issue in BEC modeling.*

We agree the statement may be confusing, and modified it in the revision.

## Response to the comments of Referee #2

We are grateful to the reviewer for his careful reading of the paper. The reviewer's comments helped us greatly to improve the presentation of our ideas and results. In what follows, we repeat each of the reviewer's comments in italic, and provide our response in roman.

*In most implementations of the Ensemble Kalman Filter (EnKF), ensemble covariances between distinct variables defined at the same location in space-time are not attenuated. This paper successfully makes the point that, in some circumstances, EnKF performance would be improved by attenuating such inter-variable correlations.*

*The paper identifies simple ensemble covariance attenuation strategies for covariances between variables of different types such as zonal wind and temperature. The proposed strategies all guarantee the symmetry and semi-positive definiteness of the localized covariance matrix. The utility of the proposed approaches is evaluated using an idealized chaotic system with fast and slow variables. For this particular system and a fairly dense observing network, it is found that attenuating the inter-variable ensemble covariances improves EnKF performance.*

*The inter-variable covariance attenuation methods given by equations (6)-(9) and the associated discussion appear to pertain to the case when there are just two distinct variables at each grid-point. The paper would be of greater interest if corresponding formulae were given for the general case where there were  $M$  distinct variables at each model grid point.*

We appreciate the reviewer's comments. We agree with the reviewer that extending to a more general case with  $M$  distinct variables is useful. We now give a general formula for arbitrary number of variables in Eqs. (8) and (11) of the revision.

*The numerical experiments performed in this paper would be more informative if an effort had been made to establish the magnitude of the true error correlations between the slow ( $X$ ) and fast ( $Y$ ) variables in the system considered. It is only when that number is known that the potential gain of not zeroing out the inter-variable correlations can be quantified.*

We calculated the cross-correlation between  $X$  and  $Y$  variables with 500 samples drawn from the model (without assimilation) and thus this cross-correlation can be considered as the true cross-correlation between the two variables. The magnitude varies between  $-0.4$  and  $0.4$ , thus the correlation between two variables seems quite strong. We added this statement in the

revision.

*Another issue the authors might aim for in revising their paper is to come up with some rules of thumb to predict from the true error correlation and known random ensemble size when (a) there would be little to be gained in attenuating inter-variable ensemble correlations, or (b) there would be little to be gained in keeping any of the inter-variable ensemble correlation, or (c) partial attenuation of the inter-variable correlations would be helpful.*

We appreciate the reviewer's comments. We agree that this is a great point, but given the limited time frame, we could only add an experiment with 500 ensemble members, under the same setting as the experiment with 20 ensemble members. Based on our additional experiment, we see that, in the bivariate Lorenz-95 model case (which shows non negligible cross-correlation between the two state variables), accounting for cross-correlation and at the same time partially attenuating cross-correlation give the best result. By trying various  $\beta$  values, we attempted to pick the best amount of partial-attenuation of cross-correlation.

*3. As a check on the EnKF code and to quantify the upper limit of the usefulness of  $X$ - $Y$  covariances, I think the paper would be stronger if you added another experiment in which the ensemble size was 16 to 32 times larger than the 40 member ensemble you considered here. With that experiment, you should be able to isolate the data assimilation value of accurately estimating  $X$ - $Y$  covariances.*

We appreciate this comment and we agree that suggested experiment can give us more insight. However, as indicated in the previous response, we could only add an experiment with 500 ensemble members.

*4. The conclusions need to admit that the found superiority of the Askey localization function over the Gaspari-Cohn localization function may not extend to other chaotic models or observation networks. Askey might be better when the true correlation function looks more like the Askey function than the Gaspari-Cohn function and vice-versa?*

We agree with your comment, and added in Discussion section that the Askey function may not be superior to the Gaspari-Cohn function in other models, and that which correlation function is better depends on what the true correlation function looks like.

*Minor Specific Comments: 5. Abstract, line 8: Change ?entry-wise? to*

?element-wise?.

Done.

6. *Equation (2): Most EnKFs do not use the linearized observation operator in the definition of the gain. Thus, (2) or the discussion around it needs to be changed so that the reader is fully aware of the EnKF's ability to directly estimate covariances between forecasts of variables that are non-linear functions of the state and the state variables themselves.*

We put the following sentence instead of avoiding the use of “linearization”. EnKF schemes usually avoid the explicit computation of the linearized observation operator  $\mathbf{H}$  by using approximations to  $\mathbf{P}^b\mathbf{H}^T$  and  $\mathbf{H}\mathbf{P}^b\mathbf{H}^T$  that involve only the computation of  $h(\mathbf{x}^b)$  and  $\bar{h}(\mathbf{x}^b)$  (e.g., Houtekamer and Mitchell 1998).

7. *P843, line 14. To more clearly define s give an example e.g ?if the state is defined at a particular instant on a latitude, longitude, height grid then s=3? ? if that's what you mean.*

We added that if the state is defined at a particular instant on a grid formed by latitude, longitude, and height, then s=3.

8. *Equations (12) and (13): The relationship between this model and model 3 of Lorenz (2005, JAS) needs to be pointed out.*

We compared the two models in the beginning of Section 3.b.

9. *P847., lines 6-11. I think it would be clearer if you replaced “cross-covariances are set to zero” with “covariances between X and Y variables are set to zero” if if that's what you mean. Also, I'm not sure what you mean by “marginal covariances”. Do you mean X-X and Y-Y covariances? Please clarify these issues in the revised text.*

Cross-covariance and marginal covariance are defined in Section 2.b, but we replaced the terms as suggested by the reviewer.

10. *Very little was said about Figures 8-11. Either discuss each one individually or replace some of them with a summary statement of what they indicate.*

We replaced this with the results with 500-member ensemble with discussion about the results.

<sup>1</sup> **Multivariate Localization Methods for Ensemble Kalman Filtering**

<sup>2</sup> **SOOJIN ROH**

*Department of Statistics, Texas A&M University, College Station, TX, USA*

<sup>3</sup> **MIKYOUNG JUN\***

*Department of Statistics, Texas A&M University, College Station, TX, USA*

<sup>4</sup> **ISTVAN SZUNYOGH**

*Department of Atmospheric Sciences, Texas A&M University, College Station, TX, USA*

<sup>5</sup> **MARC G. GENTON**

*CEMSE Division, King Abdullah University of Science and Technology, Thuwal, Saudi Arabia*

---

\*Corresponding author address: 3143 TAMU, College Station, TX 77843-3143 USA.  
Email:mjun@stat.tamu.edu

## ABSTRACT

7 In ensemble Kalman filtering (EnKF), the small number of ensemble members that is feasible to  
8 use in a practical data assimilation application leads to sampling variability of the estimates of the  
9 background error covariances. The standard approach to reducing the effects of this sampling  
10 variability, which has also been found to be highly efficient in improving the performance of  
11 EnKF, is the localization of the estimates of the covariances. One family of localization techniques  
12 is based on taking the Schur (**element**-wise) product of the ensemble-based sample covariance  
13 matrix and a correlation matrix whose entries are obtained by the discretization of a distance-  
14 dependent correlation function. While the proper definition of the localization function for a  
15 single state variable has been extensively investigated, a rigorous definition of the localization  
16 function for multiple state variables has been seldom considered. This paper introduces two  
17 strategies for the construction of localization functions for multiple state variables. The proposed  
18 localization functions are tested by assimilating simulated observations experiments into the  
19 bivariate Lorenz 95 model with their help.

20 **1. Introduction**

21 The components of the finite-dimensional state vector of a numerical model of the atmosphere  
22 are defined by the spatial discretization of the state variables considered in the model. An  
23 ensemble-based Kalman filter (EnKF) data assimilation scheme treats the finite-dimensional  
24 state vector as a multivariate random variable and estimates its probability distribution by an  
25 ensemble of samples from the distribution. To be precise, an EnKF scheme assumes that the  
26 probability distribution of the state is described by a multivariate normal distribution and it  
27 estimates the mean and the covariance matrix of that distribution by the ensemble (sample)  
28 mean and the ensemble (sample) covariance matrix. The estimate of the mean and the estimate  
29 of the covariance matrix of the analysis distribution are obtained by updating the mean and the  
30 covariance matrix of a background (prior) distribution based on the latest observations. The  
31 background distribution is represented by an ensemble of short-term forecasts from the previous  
32 analysis time. This ensemble is called the background ensemble.

33 Because the number of background ensemble members that is feasible to use in a realistic  
34 atmospheric model is small, the estimates of weak covariances (the entries with small absolute  
35 values in the background covariance matrix) tend to have large relative estimation errors. These  
36 large relative errors have a strong negative effect on the accuracy of an EnKF estimate of the  
37 analysis mean. The standard approach to alleviating this problem is to apply a physical-distance-  
38 dependent localization to the sample background covariances before their use in the state update  
39 step of the EnKF. In essence, localization is a method to introduce the empirical understand-  
40 ing that the true background covariances tend to rapidly decrease with distance into the state  
41 estimation process.

42 Data assimilation schemes treat the spatially discretized state vector,  $\mathbf{x}$ , as a multivariate

43 random variable. We use the conventional notation  $\mathbf{x}^b$  and  $\mathbf{x}^a$  for the background and the  
 44 analysis state vectors, respectively. We also use the notation  $\mathbf{y}^\circ$  for the vector of observations.  
 45 In an EnKF scheme, the analysis mean,  $\bar{\mathbf{x}}^a$ , is computed from the background mean,  $\bar{\mathbf{x}}^b$ , by the  
 46 update equation

$$\bar{\mathbf{x}}^a = \bar{\mathbf{x}}^b + \mathbf{K} \left( \mathbf{y}^\circ - \overline{h(\mathbf{x}^b)} \right). \quad (1)$$

47 The function  $h(\cdot)$  is the observation function, which maps the finite-dimensional state vector  
 48 into observables. Thus,  $\overline{h(\mathbf{x}^b)}$  is the ensemble mean of the prediction of the observations by the  
 49 background. The matrix

$$\mathbf{K} = \mathbf{P}^b \mathbf{H}^T \left( \mathbf{H} \mathbf{P}^b \mathbf{H}^T + \mathbf{R} \right)^{-1} \quad (2)$$

50 is the Kalman gain matrix, where  $\mathbf{P}^b$  is the background covariance matrix,  $\mathbf{H}$  is the linearization  
 51 of  $h$  about  $\bar{\mathbf{x}}^b$ , and  $\mathbf{R}$  is the observation error covariance matrix. EnKF schemes usually avoid  
 52 the explicit computation of the linearized observation operator  $\mathbf{H}$  by using approximations to  
 53  $\mathbf{P}^b \mathbf{H}^T$  and  $\mathbf{H} \mathbf{P}^b \mathbf{H}^T$  that involve only the computation of  $h(\mathbf{x}^b)$  and  $\overline{h(\mathbf{x}^b)}$  (e.g., Houtekamer and  
 54 Mitchell 1998). The entry  $K_{ij}$  of  $\mathbf{K}$  determines the effect of the  $j$ -th observation on the  $i$ -th  
 55 component of the analysis mean,  $\bar{\mathbf{x}}^a$ . Under the standard assumption that the observation errors  
 56 are uncorrelated, the matrix,  $\mathbf{R}$ , is diagonal. Hence, the way the effect of the observations is  
 57 spread from the observations to the different locations and state variables is determined by  $\mathbf{P}^b$   
 58 and  $\mathbf{H}$ . The sampling variability in the estimates of  $\mathbf{P}^b$  affects the accuracy of the information  
 59 propagated in space and between the different state variables through the matrix products,  $\mathbf{P}^b \mathbf{H}^T$   
 60 and  $\mathbf{H} \mathbf{P}^b \mathbf{H}^T$ . The goal of localization is to reduce the related effects of sampling variability on  
 61 the estimates of  $\mathbf{K}$ .

62 Over the years, many different localization methods have been proposed. Hamill et al. (2001),  
 63 Houtekamer and Mitchell (1998, 2001), Hunt et al. (2007), Ott et al. (2004), and Whitaker and

64 Hamill (2002) used localization functions which set the covariance to zero beyond a certain  
65 distance (localization radius). Jun et al. (2011) proposed a nonparametric statistical method to  
66 estimate the covariance. Anderson (2007) used a hierarchical ensemble filter which estimates the  
67 covariance using an ensemble of ensemble filters. Bishop and Hodyss (2007, 2009a,b) adaptively  
68 determined the width of localization by computing powers of the sample correlations. Buehner  
69 and Charron (2007) examined the spectral and spatial localization of error covariance. Anderson  
70 and Lei (2013) and Lei and Anderson (2014) proposed an empirical localization function based  
71 on the output of an observing system simulation experiment.

72 The focus of the present paper is on the family of schemes that localize the covariances  
73 by taking the Schur (Hadamard) product of the sample background covariance matrix and a  
74 correlation matrix of the same size, whose entries are obtained by the discretization of a distance-  
75 dependent correlation function with local (compact) support (e.g., Hamill et al. 2001; Houtekamer  
76 and Mitchell 2001; Whitaker and Hamill 2002). Such a correlation function is usually called a  
77 *localization* or *taper function*. The commonly used localization functions were introduced by  
78 Gaspari and Cohn (1999). Beyond a certain distance, all localization functions become zero,  
79 forcing the filtered estimates of the background covariance between state variables at locations  
80 that are far apart in space to zero. This property of the filtered background covariances can also  
81 be exploited to increase the computational efficiency of the EnKF schemes.

82 Eqs. (1) and (2) provide the solution of a formulation of the data assimilation problem  
83 that assumes that  $\mathbf{P}^b$  is invertible (e.g., sections 4.2.1 and 4.2.3 of Szunyogh 2014). A realistic  
84 atmospheric model has multiple scalar state variables (e.g., temperature, coordinates of the wind  
85 vector, surface pressure, humidity). If a univariate localization function, such as that described  
86 by Gaspari and Cohn (1999), is applied directly to a multivariate state vector, the resulting  
87 localized background covariance matrix may not be positive-definite. Because  $\mathbf{P}^b$  is symmetric,

88 its eigenvalues are real and non-negative, which implies that it is invertible, only if it is also  
89 positive-definite. (An  $n \times n$  symmetric matrix  $\mathbf{A}$  is positive-definite if  $\mathbf{x}^T \mathbf{A} \mathbf{x} > 0$  for all non-zero  
90 vectors  $\mathbf{x} \in \mathbb{R}^n$ .) Because the computation of the right-hand-side of Eq. (2) does not require  
91 the invertibility of  $\mathbf{P}^b$ , singularity of the localized  $\mathbf{P}^b$  usually does not lead to a breakdown  
92 of the computations in practice. An ill-conditioned estimate of  $\mathbf{P}^b$ , however, can degrade the  
93 conditioning (increase the condition number) of  $\mathbf{H} \mathbf{P}^b \mathbf{H}^T + \mathbf{R}$ , making the numerical computation  
94 of the right-hand side of Eq. (2) less stable. This motivates us to seek rigorously-derived  
95 multivariate localization functions for ensemble Kalman filtering. As will be demonstrated, such  
96 rigorously-derived multivariate localization functions often produce more accurate analyses than  
97 those that apply the same univariate localization functions to each scalar component of the  
98 state vector. Kang et al. (2011) also introduced a multivariate localization method that zeros  
99 out covariances between physically unrelated variables. Their motivation for zeroing out such  
100 covariances, however, was to filter apparent spurious covariances rather than to preserve the  
101 positive-definiteness of the background error covariance matrix.

102 In our search for proper multivariate localization functions, we take advantage of recent  
103 developments in the statistics literature. In particular, we use the localization functions developed  
104 in Porcu et al. (2012), who studied the radial basis functions to construct multivariate correlation  
105 functions with compact support. Note that Section 5 in Zhang and Du (2008) described a general  
106 methodology for covariance tapering in the case of multiple state variables. Du and Ma (2013)  
107 used a convolution approach and a mixture approach to derive covariance matrix functions  
108 with compactly supported covariances. Kleiber and Porcu (2015) constructed nonstationary  
109 correlation functions with compact support for multivariate random fields. Genton and Kleiber  
110 (2015) reviewed approaches to building models for covariances between two different variables  
111 such as compactly supported correlation functions for multivariate Gaussian random fields.

112 The rest of the paper is organized as follows. Section 2 briefly describes EnKF and localization  
113 for the special case of two state variables. Section 3 describes the bivariate Lorenz-95 model we  
114 use to test our ideas. Section 4 summarizes the main results of the paper.

## 115 2. Methodology

### 116 a. Univariate localization

117 In principle, localization can be implemented by using filtered estimates of the background  
118 covariances rather than the raw sample covariances to define the matrix,  $\mathbf{P}^b$ , used in the compu-  
119 tation of  $\mathbf{K}$  by Eq. (2). The filtered (localized) version of covariance matrix,  $\tilde{\mathbf{P}}^b$ , is obtained by  
120 computing the Schur (*element*-wise) product:

$$\tilde{\mathbf{P}}^b = \hat{\mathbf{P}}^b \circ \mathbf{C}, \quad (3)$$

121 where  $\mathbf{C}$  is a correlation matrix, which has the same dimensions as the sample covariance matrix,  
122  $\hat{\mathbf{P}}^b$ . In practice, however, the localization is often done by taking advantage of the fact that  
123 localization affects the analysis through  $\mathbf{P}^b \mathbf{H}^T$  and  $\mathbf{H} \mathbf{P}^b \mathbf{H}^T$ , or, ultimately, through  $\mathbf{K}$ . In  
124 particular, because a distance,  $d$ , can be defined for each entry,  $K_{ij}$ , of  $\mathbf{K}$  by the distance  
125 between the  $i$ -th analyzed variable and the  $j$ -th observation, the simplest localization strategy is  
126 to set all entries,  $K_{ij}$ , that are associated with a distance longer than a prescribed localization  
127 radius,  $R$  ( $d > R$ ), to zero, while leaving the remaining entries unchanged (e.g., Houtekamer and  
128 Mitchell 1998; Ott et al. 2004; Hunt et al. 2007).

129 Another approach is to localize  $\mathbf{P}^b \mathbf{H}^T$  and  $\mathbf{H} \mathbf{P}^b \mathbf{H}^T$  by a tapering function (e.g., Hamill et al.

130 2001; Houtekamer and Mitchell 2001). The usual justification for this approach is that  $\mathbf{H}$  is  
131 typically the linearization of a local interpolation function,  $h(\cdot)$ , for which the localized matrix  
132 products provide good approximations of the products computed by using localized estimates of  
133  $\mathbf{P}^b$ . Note that  $\mathbf{P}^b \mathbf{H}^T$  is the matrix of background covariances between the state variables at the  
134 model grid points and at the observation locations, while  $\mathbf{H} \mathbf{P}^b \mathbf{H}^T$  is the matrix of background  
135 covariances between the state variables at the observation locations. Thus, a distance can be  
136 associated with each entry of the two matrix products, which makes the distance-dependent  
137 localization of the two products possible. The approach becomes problematic, however, when  
138  $h(\cdot)$  is not a local function, which is the typical case for remotely sensed observations (Campbell  
139 et al. 2010).

140 We consider the situation where localization is applied directly to the background error co-  
141 variance matrix,  $\hat{\mathbf{P}}^b$ . Recall that the localized covariance matrix is expressed as in Eq. (3). In  
142 particular,  $\mathbf{C}$  is a positive-definite matrix with strictly positive eigenvalues, while the sample  
143 covariance matrix,  $\hat{\mathbf{P}}^b$ , may have zero eigenvalues (as it is only non-negative definite). The lo-  
144 calization in (3) helps to eliminate those zero eigenvalues of  $\hat{\mathbf{P}}^b$  and **alleviates** the related large  
145 relative estimation errors. The positive-definiteness of  $\mathbf{C}$  ensures that localization does not in-  
146 troduce new zero eigenvalues in the process of eliminating the zero eigenvalues of  $\hat{\mathbf{P}}^b$ . The proper  
147 definition of the localization function that ensures that  $\mathbf{C}$  is positive-definite has been thoroughly  
148 investigated for the univariate case ( $N = 1$ ) in the literature (e.g. Gaspari and Cohn (1999)).

149 *b. Multivariate localization*

150 We now consider a model with **multiple state variables ( $N > 1$ )**. For instance, we take a  
151 simple model based on the hydrostatic primitive equations. This model solves the equations

152 for the two horizontal components of wind, the surface pressure, the virtual temperature and a  
 153 couple of atmospheric constituents. The state of the model is represented by the state vector,  
 154  $\mathbf{x} = (\mathbf{x}_1, \mathbf{x}_2, \dots, \mathbf{x}_N)$ , where  $\mathbf{x}_i$ ,  $i = 1, 2, \dots, N$ , represents the spatially discretized state of the  
 155  $i$ -th state variable in the model.

156 The sample background covariance matrix,  $\hat{\mathbf{P}}^b$ , can be partitioned as

$$\hat{\mathbf{P}}^b = \begin{pmatrix} \hat{\mathbf{P}}_{11}^b & \hat{\mathbf{P}}_{12}^b & \dots & \hat{\mathbf{P}}_{1N}^b \\ \hat{\mathbf{P}}_{21}^b & \hat{\mathbf{P}}_{22}^b & \dots & \hat{\mathbf{P}}_{2N}^b \\ \vdots & \vdots & \ddots & \vdots \\ \hat{\mathbf{P}}_{N1}^b & \hat{\mathbf{P}}_{N2}^b & \dots & \hat{\mathbf{P}}_{NN}^b \end{pmatrix}. \quad (4)$$

157 The entries of the submatrices,  $\hat{\mathbf{P}}_{ii}^b$ ,  $i = 1, \dots, N$ , are **called** the marginal-covariances for the  
 158  $i$ -th state variable. In practical terms, if the  $i$ -th state variable is the virtual temperature, for  
 159 instance, each diagonal entry of  $\hat{\mathbf{P}}_{ii}^b$  represents the sample variance for the virtual temperature at  
 160 a given model grid point, while each off-diagonal entry of  $\hat{\mathbf{P}}_{ii}^b$  represents the sample covariances  
 161 between the virtual temperatures at a pair of grid points. Likewise, the entries of  $\hat{\mathbf{P}}_{ij}^b$ ,  $i \neq j$ , are  
 162 **called** the sample cross-covariances between the grid point values of the  $i$ -th and the  $j$ -th state  
 163 variables at pairs of locations, where the two locations for an entry can be the same grid point.

164 We thus consider matrix-valued localization functions,  $\boldsymbol{\rho}(d) = \{\rho_{ij}(d)\}_{i,j=1,\dots,N}$ , which are  
 165 continuous functions of  $d$ . The component  $\rho_{ij}(d)$  of  $\boldsymbol{\rho}(d)$  is the localization function used for  
 166 the calculation of the covariances included in the sub-matrix  $\mathbf{P}_{ij}^b$  of  $\mathbf{P}^b$ . Each entry of the  
 167 localization matrix  $\mathbf{C}$  is computed by considering the value of the appropriate component of  
 168  $\boldsymbol{\rho}(d)$  for a particular pair of state variables and the distance,  $d$ , associated with the related entry  
 169 of  $\hat{\mathbf{P}}^b$ .

170 In order to get a proper matrix-valued localization function,  $\rho$ , a seemingly obvious approach  
 171 to extend the results of Gaspari and Cohn (1999) would be to compute the entries of  $\mathbf{C}$  based  
 172 on a univariate correlation function for a multivariate variable. That is, for the pair of state  
 173 variables  $i$  and  $j$ , we localize the corresponding sample background covariance matrix,  $\hat{\mathbf{P}}_{ij}^b$ , by  
 174 multiplying a localization matrix from the same correlation function for all  $i$  and  $j$ . Formally,  
 175 this would be possible because the distance  $d$  is uniquely defined for each entry of  $\hat{\mathbf{P}}^b$  the same  
 176 way in the multivariate case as in the univariate case. This approach, however, cannot guarantee  
 177 the positive-definiteness of the resulting matrix,  $\mathbf{C}$ . As a simple illustrative example, consider  
 178 the situation where the discretized state vector has only two components that are defined by  
 179 two different scalar state variables at the same location (e.g., the temperature and the pressure).  
 180 In this case, if  $n$  is the number of locations, the localization matrix for the two state variables  
 181 together can be written as

$$\mathbf{C} = \begin{pmatrix} \mathbf{C}_0 & \mathbf{C}_0 \\ \mathbf{C}_0 & \mathbf{C}_0 \end{pmatrix} \quad (5)$$

182 independently of the particular choice of the localization function. Here  $\mathbf{C}_0$  is an  $n \times n$  localization  
 183 matrix from a univariate localization function. From Eq. (5), it is clear that  $n$  eigenvalues of  $\mathbf{C}$   
 184 are zero and the rank of  $\mathbf{C}$  is  $n$ , while its dimension is  $2n \times 2n$ .

185 As in Eq. (2), although  $\mathbf{C}$  is rank-deficient and thus so is the localized covariance matrix  
 186  $\tilde{\mathbf{P}}^b$ , we may still be able to calculate the inverse of  $\mathbf{H}\tilde{\mathbf{P}}^b\mathbf{H}^T + \mathbf{R}$ , as  $\mathbf{R}$  is a diagonal matrix.  
 187 The smallest eigenvalue of  $\mathbf{H}\tilde{\mathbf{P}}^b\mathbf{H}^T + \mathbf{R}$  is the smallest (positive) value of  $\mathbf{R}$ , and thus the  
 188 matrix,  $\mathbf{H}\tilde{\mathbf{P}}^b\mathbf{H}^T + \mathbf{R}$ , is still invertible and has positive eigenvalues. However, unless the diagonal  
 189 elements of  $\mathbf{R}$  are large (which implies large observation error variance), the matrix  $\mathbf{H}\tilde{\mathbf{P}}^b\mathbf{H}^T + \mathbf{R}$   
 190 is seriously ill-conditioned and the computation of its inverse may be numerically unstable.  
 191 Therefore, the numerical stability of the computation of the inverse of the matrix heavily relies

192 on the observation error variance, which is an undesirable property.

193 We therefore propose two approaches to construct positive-definite (full rank) matrix-valued  
 194 localization functions,  $\rho(d)$ . The first proposed method takes advantage of the knowledge of  
 195 a proper univariate localization function,  $\tilde{\rho}$ . Instead of using the same correlation function to  
 196 localize multiple state variables, for a certain distance lag, we let  $\rho = \tilde{\rho} \cdot \mathbf{B}$ , where  $\mathbf{B}$  is an  $N \times N$   
 197 symmetric, positive-definite matrix whose diagonal entries are one. It can be easily verified that  
 198  $\rho$  is a matrix-valued positive-definite function, which makes it a valid multivariate localization  
 199 function. For instance, in the hypothetical case where the two components of the state vector  
 200 are two different state variables at the same location, making the choice

$$\mathbf{B} = \begin{pmatrix} 1 & \beta \\ \beta & 1 \end{pmatrix}, \quad (6)$$

201 for  $\beta$  with  $|\beta| < 1$ , leads to

$$\mathbf{C} = \begin{pmatrix} \mathbf{C}_0 & \beta\mathbf{C}_0 \\ \beta\mathbf{C}_0 & \mathbf{C}_0 \end{pmatrix} \quad (7)$$

202 rather than what is given in Eq. (5). Since the eigenvalues of the matrix  $\mathbf{B}$  are  $1 \pm \beta > 0$ , it  
 203 can be easily verified that the matrix in (7) is positive-definite. For the case with more than two  
 204 state variables ( $N \geq 3$ ), the matrix  $\mathbf{B}$  can be parametrized as  $\mathbf{B} = \mathbf{L}\mathbf{L}^T$ , where

$$\mathbf{L} = \begin{bmatrix} \ell_{1,1} & 0 & \cdots & 0 \\ \ell_{2,1} & \ell_{2,2} & \cdots & 0 \\ \vdots & \vdots & \ddots & 0 \\ \ell_{N,1} & \ell_{N,2} & \cdots & \ell_{N,N} \end{bmatrix} \quad (8)$$

205 is a lower triangular matrix with the constraints that  $\sum_{j=1}^i \ell_{i,j}^2 = 1$  and  $\ell_{i,i} > 0$  for all  $i =$   
 206  $1, \dots, N$ . The constraints are used to have the diagonal entries of  $\mathbf{B}$  to be one. Furthermore, we  
 207 need the constraint that for each row of  $\mathbf{L}$ , the sum of all of the squared elements should be 1 in  
 208 order to have the diagonal entries of  $\mathbf{B}$  to be one. Other than these constraints, the elements of  
 209  $\mathbf{L}$  can vary freely in order to guarantee the positive-definiteness of  $\mathbf{B}$ .

210 An attractive feature of this approach is that we can take advantage of any known univariate  
 211 localization function to produce a multivariate localization function. However, the multivariate  
 212 localization function from this approach is *separable* in the sense that the multivariate component  
 213 (i.e.,  $\mathbf{B}$ ) and the localization function (i.e.  $\tilde{\rho}$ ) are factored. Another limitation of the approach is  
 214 that the localization radius and decay rate are the same for each pair of state variables, leaving  
 215 no flexibility to account for the potential differences in the correlation lengths and decay rate for  
 216 the different state vector components.

217 The second proposed method takes advantage of the availability of multivariate compactly  
 218 supported functions from the spatial statistics literature. To the best of our knowledge, only a  
 219 few papers have been published on this subject; one of them is Porcu et al. (2012). The function  
 220 class they considered was essentially a multivariate extension of the *Askey* function (Askey 1973),  
 221  $f(d; \nu, c) = (1 - \frac{d}{c})_+^\nu$ , with  $c, \nu > 0$ . Here,  $x_+ = \max(x, 0)$  for  $x \in \mathbb{R}$ . For instance, a bivariate  
 222 Askey function, which is a special case of the results of Porcu et al. (2012), is given by ( $i, j = 1, 2$ )

$$\rho_{ij}(d; \nu, c) = \beta_{ij} \left(1 - \frac{d}{c}\right)_+^{\nu + \mu_{ij}}, \quad (9)$$

223 where  $c > 0$ ,  $\mu_{12} = \mu_{21} \leq \frac{1}{2}(\mu_{11} + \mu_{22})$ ,  $\nu \geq [\frac{1}{2}s] + 2$ ,  $\beta_{ii} = 1$  ( $i = 1, 2$ ),  $\beta_{12} = \beta_{21}$ , and

$$|\beta_{12}| \leq \frac{\Gamma(1 + \mu_{12})}{\Gamma(1 + \nu + \mu_{12})} \sqrt{\frac{\Gamma(1 + \nu + \mu_{11})\Gamma(1 + \nu + \mu_{22})}{\Gamma(1 + \mu_{11})\Gamma(1 + \mu_{22})}}. \quad (10)$$

224 Here,  $\Gamma(\cdot)$  is the gamma function (e.g., Wilks 2006),  $s$  is the dimension of the Euclidean space  
 225 where the state variable is defined. If the state is defined at a particular instant on a grid formed  
 226 by latitude, longitude, and height, then  $s = 3$ . Here,  $[x]$  is the largest integer that is equal to or  
 227 smaller than  $x$ . The Askey function in (9) has the support  $c$  because it sets covariances beyond  
 228 a distance  $c$  to zero. It can be seen from (10) that, if the scalars,  $\mu_{ij}$ , are chosen to be the same  
 229 for all values of  $i$  and  $j$ , the condition on  $\beta_{12}$  for  $\rho$  to be valid is  $|\beta_{12}| \leq 1$ . Note that For this  
 230 choice, the second method is essentially the same as the first method with the Askey function  
 231 set to  $\tilde{\rho}$ . The localization function given by (9) is more flexible than the functions of the first  
 232 method with the Askey function set to  $\tilde{\rho}$  because  $\mu_{ij}$  can be chosen to be different for each pair  
 233 of indexes,  $i$  and  $j$ . The localization length, however, is still the same for the different pairs of  
 234 the state variables. The multivariate Askey function is formed by

$$\rho_{ij}(d; \nu, c) = c^{\nu+1} B(\mu_{ij} + 1, \nu + 1) \left(1 - \frac{|d|}{c}\right)^{\nu+\mu_{ij}+1}, \quad |d| < c \quad (11)$$

235 and 0 otherwise, where  $\nu \geq (s + 1)/2$ ,  $\mu_{ij} = (\mu_i + \mu_j)/2$ , and  $\mu_i > 0$  for all  $i = 1, \dots, N$ . Here,  
 236  $B$  is the beta function (Porcu et al. 2012; Genton and Kleiber 2015).

237 To illustrate the differences between the shape of the Gaspari-Cohn and the Askey functions,  
 238 we show the Gaspari-Cohn function for  $c = 25$  and the univariate Askey function for  $c = 50$ ,  
 239 and  $\nu = 1, \dots, 4$  (Fig. 1). This figure shows that for a given support, the Askey functions are  
 240 narrower.

241 **3. Experiments**

242 *a. The EnKF Scheme*

243 There are many different formulations of the EnKF update equations, which produce not  
244 only an updated estimate of the mean, but also the ensemble of analysis perturbations that are  
245 added to the mean to obtain an ensemble of analyses. This ensemble of analyses serves as the  
246 ensemble of initial conditions for the model integration that produce the background ensemble.  
247 In our experiments, we use the method of perturbed observations. It obtains the analysis mean  
248 and the ensemble of analysis perturbations by the equations

$$\bar{\mathbf{x}}^a = \bar{\mathbf{x}}^b + \mathbf{K}(\mathbf{y} - \mathbf{H}\bar{\mathbf{x}}^b), \quad (12)$$

$$\mathbf{x}_k^{a'} = \mathbf{x}_k^{b'} + \mathbf{K}(\mathbf{y}_k^{o'} - \mathbf{H}\mathbf{x}_k^{b'}), \quad (13)$$

249 where  $\mathbf{x}_k'$ ,  $k = 1, 2, \dots, M$  are the ensemble perturbations and  $\mathbf{y}_k^{o'}$ ,  $k = 1, 2, \dots, M$  are random  
250 draws from the probability distribution of observation errors. As the notation suggests, we  
251 consider a linear observation function in our experiments. This choice is made for the sake of  
252 simplicity and limits the generality of our findings much less than the use of an idealized model  
253 of atmospheric dynamics.

254 For the case of multiple state variables, the ensemble members are considered to be in a single  
255 ensemble, that is, not being grouped into distinct sub-ensembles.

256 *b. The Bivariate Lorenz Model*

257 Lorenz (1995) discussed the bivariate Lorenz-95 model, which mimics the nonlinear dynamics

258 of two linearly coupled atmospheric state variables,  $X$  and  $Y$ , on a latitude circle. This model  
 259 provides a simple and conceptually satisfying representation of basic atmospheric processes, but  
 260 is not suitable for some atmospheric processes. The model 3 in Lorenz (2005) made it more  
 261 realistic and suitable with sacrifice of simplicity, by producing a rapidly varying small-scale  
 262 activity superposed on the smooth large-scale waves. We use the Lorenz-95 model for simplicity  
 263 in our following experiments.

264 The idealized model we use is the bivariate Lorenz-95 model (Lorenz 1995). The model mim-  
 265 ies the nonlinear dynamics of two linearly coupled atmospheric state variables,  $X$  and  $Y$ , on a  
 266 latitude circle. In the bivariate Lorenz-95 model, the variable,  $X$ , is a “slow” variable represented  
 267 by  $K$  discrete values,  $X_k$ , and  $Y$  is a “fast” variable represented by  $J \times K$  discrete values. The  
 268 governing equations are

$$\frac{dX_k}{dt} = -X_{k-1}(X_{k-2} - X_{k+1}) - X_k - (ha/b) \sum_{j=1}^J Y_{j,k} + F, \quad (14)$$

$$\frac{dY_{j,k}}{dt} = -abY_{j+1,k}(Y_{j+2,k} - Y_{j-1,k}) - aY_{j,k} + (ha/b)X_k, \quad (15)$$

269 where  $Y_{j-J,k} = Y_{j,k-1}$  and  $Y_{j+J,k} = Y_{j,k+1}$  for  $k = 1, \dots, K$  and  $j = 1, \dots, J$ . The “boundary  
 270 condition” is periodic; that is,  $X_{k-K} = X_{k+K} = X_k$ , and  $Y_{j,k-K} = Y_{j,k+K} = Y_{j,k}$ . In our  
 271 experiments,  $K = 36$  and  $J = 10$ . The parameter  $h$  controls the strength of the coupling  
 272 between  $X$  and  $Y$ ,  $a$  is the ratio of the characteristic time scales of the slow motion of  $X$  to the  
 273 fast motion of  $Y$ ,  $b$  is the ratio of the characteristic amplitudes of  $X$  to  $Y$ , and  $F$  is a forcing  
 274 term. We choose the parameters to be  $a = 10$ ,  $b = 10$ ,  $F = 10$ , and  $h = 2$ . These values of the  
 275 model parameters are equal to those originally suggested by Lorenz (1995), except for the value  
 276 of the coupling coefficient  $h$ , which is twice as large in our case. We made this change in  $h$  to

277 increase the covariances between the errors in the estimates of  $X$  and  $Y$ , which makes the model  
278 more sensitive to the choices of the localization parameters. We use a fourth-order Runge-Kutta  
279 time integration scheme with a time step of 0.005 non-dimensional units as Lorenz (1995) did.  
280 We define the physical distances between  $X_{k_1}$  and  $X_{k_2}$ , between  $Y_{j_1, k_1}$  and  $Y_{j_2, k_2}$ , and between  
281  $X_{k_1}$  and  $Y_{j_1, k_2}$  by  $|10(k_1 - k_2)|$ ,  $|10(k_1 - k_2) + j_1 - j_2|$ , and  $|10(k_1 - k_2) - j_1|$ , respectively. Fig. 2  
282 shows a typical state of the model for the selected parameters. The figure shows that  $X$  tends to  
283 drive the evolution of  $Y$ : the hypothetical process represented by  $Y$  is more active (its variability  
284 is higher) with higher values of  $X$ .

285 *c. Experimental Design*

286 Since the estimates of the cross-covariances play a particularly important role at locations  
287 where one of the variables is unobserved, we expect an improved treatment of the cross-  
288 covariances to lead to analysis improvements at locations where only one of the state variables is  
289 observed. This motivates us to consider an observation scenario in which  $X$  and  $Y$  are partially  
290 observed. The variable  $X$  is observed at randomly chosen 20% of all locations and  $Y$  is observed  
291 at randomly chosen 90% of those locations where  $X$  is not observed. Spatial locations of the  
292 partially observed  $X$  and  $Y$  are illustrated in Fig. 3. The results from this experiment are  
293 compared to those from a control experiment, in which both  $X$  and  $Y$  are fully observed.

294 We first generate a time series of “true” model states by a 2,000-time-step integration of  
295 the model. We initialize an ensemble by adding the standard Gaussian noise to the true state;  
296 then, discarding the first 3,000 time steps. We then generate simulated observations by adding  
297 random observation noise of mean zero and variance 0.02 to the the appropriate components  
298 of the “true” state of  $X$  at each time step. We use the same procedure to generate simulated

299 observations of  $Y$ , except that the variance of the observation noise is 0.005. Observations are  
 300 assimilated at every time step by first using a 20-member ensemble with a constant covariance  
 301 inflation factor of 1.015. The error in the analysis at a given verification time is measured by  
 302 the root-mean-square distance between the analysis mean and the true state. We refer to the  
 303 resulting measure as the root-mean-square error (RMSE). The probability distribution of the  
 304 RMSE for the last 1,000 time steps of 50 different realizations of each experiment is shown by a  
 305 boxplot. The boxplot is an effective way of displaying a summary of the distribution of numbers.  
 306 The lower and upper bounds of the box respectively give the 25th and 75th percentiles. The  
 307 thick line going across the interior of the box gives the median. The whisker depends on the  
 308 interquartile range (IQR) that is precisely equal to the vertical length of the box. The whiskers  
 309 extend to the extreme values which are no more than 1.5 IQR from the box. Any values that fall  
 310 outside of the end points of whiskers are considered outliers and they are displayed as circles.

311 In the boxplot figures in the next section, we compare the RMSE for four different localization  
 312 schemes. We use the following notation to distinguish between them in the figures:

- 313 i. S1—the bivariate sample background covariance is used without localization;
- 314 ii. S2—same as S1 except that the cross-covariances between  $X$  and  $Y$  are replaced by zeros;
- 315 iii. S3—a univariate localization function is used to filter the marginal covariances within  $X$   
 316 and  $Y$ , respectively, while the cross-covariances between  $X$  and  $Y$  are replaced by zeros;
- 317 iv. S4—one of the bivariate localization methods described in Section 2.b is used to filter both  
 318 the marginal- and the cross-covariances.

319 In the experiments identified by S4, we consider two different bivariate localization functions:  
 320 The first one is  $\rho^{(1)}(\cdot) = \{\beta_{ij}\rho^{(1)}(\cdot)\}_{i,j=1,2}$  with  $\beta_{ii} = 1$  ( $i = 1, 2$ ) and  $\beta_{ij} = \beta$  ( $i \neq j$ ) for some  $\beta$

321 such that  $|\beta| < 1$ . We use the fifth-order piecewise-rational function of Gaspari and Cohn (1999)  
 322 to define the univariate correlation function,  $\rho^{(1)}$ , in the following form,

$$\rho^{(1)}(d; c) = \begin{cases} -\frac{1}{4}(|d|/c)^5 + \frac{1}{2}(d/c)^4 + \frac{5}{8}(|d|/c)^3 - \frac{5}{3}(d/c)^2 + 1, & 0 \leq |d| \leq c, \\ \frac{1}{12}(|d|/c)^5 - \frac{1}{2}(d/c)^4 + \frac{5}{8}(|d|/c)^3 + \frac{5}{3}(d/c)^2 - 5(|d|/c) + 4 - \frac{2}{3}c/|d|, & c \leq |d| \leq 2c, \\ 0, & 2c \leq |d|. \end{cases} \quad (16)$$

323 This correlation function attenuates the covariances with increasing distance, setting all the  
 324 covariances to zero beyond distance  $2c$ . So this function has the support  $2c$ . If  $|\beta| < 1$  and  $c$  is  
 325 the same for both the marginal- and the cross-covariances, the matrix-valued function,  $\rho^{(1)}$ , is  
 326 positive-definite and of full rank. We test various values of the localization parameters  $c$  and  $\beta$ ,  
 327 and present the test results in next section.

328 The second multivariate correlation function we consider,  $\rho^{(2)}$ , is the bivariate Askey function  
 329 described in Section 2.b. In particular, we use  $\mu_{11} = 0$ ,  $\mu_{22} = 2$ ,  $\mu_{12} = 1$ , and  $\nu = 3$ . According  
 330 to Eq. (10), for these choices of parameters, the one remaining parameter,  $\beta_{12}$ , must be chosen  
 331 such that  $|\beta_{12}| < 0.79$ .

332 *d. Results*

333 Figure 4 shows the distribution of RMSE for variable  $X$  for different configurations of the  
 334 localization scheme in the case where the state is only partially observed. This figure compares  
 335 the Askey function and Gaspari-Cohn function which have the same support (localization radius),  
 336 so setting all the covariances to zero beyond the same distance. We recall that because  $X$  is  
 337 much more sparsely observed than  $Y$ , we expect to see some sensitivity of the analyses of  $X$  to

338 the treatment of the cross-covariance terms. The figure confirms this expectation. A comparison  
339 of the results for configurations S1 and S2 suggests that ignoring the cross-covariances is a better  
340 strategy than to use them without localization. This conclusion does not hold once a univariate  
341 localization is applied to the marginal covariances, as using configuration S3 produces worse  
342 results than applying no localization at all (S1).

343 Figure 4 also shows that the distribution of the state estimation error is less sensitive to the  
344 choice of localization strategy for the larger values of support. Of all localization schemes, S4 with  
345  $\beta = 0.1$  performs best regardless of the localization radius: the distribution of the state estimation  
346 error is narrow with a mean value that is lower than those for the other configurations of the  
347 localization scheme. For this choice of localization scheme and  $\beta$ , the Askey function produces  
348 smaller errors than the Gaspari-Cohn function, particularly, for smaller localization radii.

349 Figure 5 is the same as Fig. 4, except for variable  $Y$  rather than for variable  $X$ . A striking  
350 feature of the results shown in this figure is that the Askey function clearly performs better  
351 than the Gaspari-Cohn function. Another obvious conclusion is that using a smaller localization  
352 radius (a lower value of support) is clearly advantageous for the estimation of  $Y$ . This result is  
353 not surprising, considering that  $Y$  is densely observed and its spatial variability is much higher  
354 than that of  $X$ . In contrast to the results for variable  $X$ , configuration S3 produces much more  
355 accurate estimates of variable  $Y$  than do configurations S1 or S2. In addition, configuration S4  
356 performs only slightly better, and only for the lowest value of support, than does configuration  
357 S3. The latter observations indicate that the marginal covariances play a more important role  
358 than do the cross-covariances in the estimation of the densely observed  $Y$ . The proper filtering  
359 of the marginal covariances can thus greatly increase the accuracy of the estimates of  $Y$ . In other  
360 words, the densely observed  $Y$  is primarily estimated based on observations of  $Y$ . Hence, the  
361 low signal-to-noise ratio for the sample estimate of the marginal covariances for  $Y$  greatly limits

362 the value of the observations of  $Y$  at longer distances.

363 Figure 6 is the same as Fig. 4, except for the case of a fully observed state. By comparing  
364 the two figures, we see that the analysis is far less sensitive to the localization radius in the fully  
365 observed case than in the partially observed case. As can be expected, the state estimates are  
366 also more accurate in the fully observed case. In the fully observed case, localization strategy  
367 S3 performs much better than do strategies S1 and S2 and similarly to S4. This result indicates  
368 that in the fully observed case,  $X$  is primarily analyzed based on observations of  $X$ , making  
369 the analysis of  $X$  more sensitive to the localization of the marginal covariances than to the  
370 localization of the cross-covariances. Similar to the partially observed case, the Askey function  
371 tends to perform better than the Gaspari-Cohn function, but the differences between the accuracy  
372 of the state estimates for the two filter functions are negligible, except for the shortest localization  
373 radius.

374 Figure 7 shows the distribution of the errors for variable  $Y$  in the fully observed case. The best  
375 results are obtained by using a short localization radius with the Askey function, even though  
376 the variability of the error is relatively large in that case. The fact that localization strategies  
377 S3 and S4 perform similarly well shows that the estimates of the cross-covariances do not play  
378 an important role in this case; that is,  $X$  is primarily estimated based on observations of  $X$ , and  
379  $Y$  is dominantly estimated based on observations of  $Y$ .

380 We also investigated the performance of EnKF with 500-member ensemble. The results for  
381 the 500-member ensemble are shown in Figures 8 to 11. We use an inflation factor of 1.005 for  
382 500 ensembles, because the optimal value of the inflation factor is typically smaller for a larger  
383 ensemble. The rank of the 500-member ensemble covariance matrix is significantly larger than  
384 that of the 20-member ensemble covariance matrix, as expected.

385 Figures 8 to 11 show that, overall, S4 still performs better than the other localization schemes

386 regardless of the choice of localization radius, as in the case of the 20-member ensemble. In  
387 particular, when observations are partially observed, S4 with  $\beta = 0.01$  provides the smallest  
388 RMSE. The cross-correlation between  $X$  and  $Y$ , calculated using 500-member ensembles without  
389 assimilating any observation, varies from  $-0.4$  to  $0.4$ , which indicates that the cross-correlation  
390 between the two variables are not negligible. Therefore, improved treatment of cross-covariance  
391 tends to lead to an improved accuracy in the state estimation.

392 The results with the 500-member ensemble also show that the distribution of the state estima-  
393 tion error is in general less sensitive to the choice of the localization function or the localization  
394 radius, compared to the 20-member ensemble case. Figure 8, however, shows that for the estima-  
395 tion of sparsely observed  $X$ , the localization scheme S3 with smaller localization radius performs  
396 worse than that with larger localization radius. For variable  $Y$  in the partially observed case  
397 (Figure 8) and both variables  $X$  and  $Y$  in the fully observed case (Figures 10 and 11), the best  
398 results are obtained with S3 and S4 regardless of the localization radius. They also shows that  
399 the state estimation error is not sensitive but stable to the choice of localization radius.

400 Figures 10 and 11 show that the localization schemes, S3 and S4, perform in a similar way,  
401 and obviously perform better than the other two localization schemes. This might imply that  
402 the cross-covariances do not have much influence on the state estimation in the fully observed  
403 case, once the covariances within each state variable are localized.

404 Figures 8–11 show the results for the 40-member ensemble. We use an inflation factor of  
405 1.005, because the optimal value of the inflation factor is typically smaller for a larger ensemble.  
406 Figure 8 shows that the ensemble size has little effect on the estimates of  $X$  in the case of the  
407 partially observed state. For variable  $Y$  in the partially observed case (Fig. 8) and both variables  
408  $X$  and  $Y$  in the fully observed case (Figs. 10 and 11), however, the best results are obtained  
409 with a larger localization radius than in the case of the 20-member ensemble. This behavior is

410 expected, as a larger ensemble can more accurately estimate the weaker covariances associated  
411 with the longer distances. As for the 20 member ensemble, the localization schemes using the  
412 Askey function perform better than those using the Gaspari-Cohn function.

## 413 4. Discussion

414 The central argument of this paper is that applying a single localization function for the  
415 localization of covariances between multiple state variables in an EnKF scheme may lead to a  
416 rank deficient estimate of the background covariance matrix. We suggested two different ap-  
417 proaches for the construction of positive-definite filtered estimates of the background covariance  
418 matrix. One of them takes advantage of the knowledge of a proper univariate localization func-  
419 tion, whereas the other uses a multivariate extension of the Askey function. The results of our  
420 numerical experiments show that a mathematically proper localization function often leads to  
421 improved state estimates. The results of the numerical experiments also suggest that of the two  
422 approaches we introduced, the one based on the Askey function produces more accurate state  
423 estimates than that based on the Gaspari-Cohn function. This fact, however, does not mean  
424 that the Askey function is always superior to the Gaspari-Cohn function in other chaotic models  
425 or observation networks. Which correlation function is superior depends on what the true error  
426 correlation looks like.

427 *Acknowledgments.*

428 The authors are grateful to the reviewers for valuable comments that significantly improved  
429 presentation of the paper. Mikyoung Jun's research was supported by NSF grant DMS-1208421,

<sup>430</sup> while Istvan Szunyogh's research was supported by ONR Grant N000140910589. This publication  
<sup>431</sup> is based in part on work supported by Award No. KUS-C1-016-04, made by King Abdullah  
<sup>432</sup> University of Science and Technology (KAUST).

## REFERENCES

435 Anderson, J. and L. Lei, 2013: Empirical localization of observation impact in ensemble kalman  
 436 filters. *Mon. Wea. Rev.*, **142**, 739–754.

437 Anderson, J. L., 2007: Exploring the need for localization in ensemble data assimilation using a  
 438 hierarchical ensemble filter. *Physica D*, **230**, 99–111.

439 Askey, R., 1973: Radial characteristic functions. technical report no. 1262, Mathematical Re-  
 440 search Center, University of Wisconsin-Madison, Madison.

441 Bishop, C. H. and D. Hodyss, 2007: Flow adaptive moderation of spurious ensemble correlations  
 442 and its use in ensemble based data assimilation. *Quart. J. Roy. Meteor. Soc.*, **133**, 2029–2044.

443 Bishop, C. H. and D. Hodyss, 2009a: Ensemble covariances adaptively localized with ECO-RAP.  
 444 Part 1: Tests on simple error models. *Tellus*, **61A**, 84–96.

445 Bishop, C. H. and D. Hodyss, 2009b: Ensemble covariances adaptively localized with ECO-RAP.  
 446 Part 2: A strategy for the atmosphere. *Tellus*, **61A**, 97–111.

447 Buehner, M. and M. Charron, 2007: Spectral and spatial localization of background-error corre-  
 448 lations for data assimilation. *Quart. J. Roy. Meteor. Soc.*, **133**, 615–630.

449 Campbell, W. F., C. H. Bishop, and D. Hodyss, 2010: Vertical covariance localization for satellite  
 450 radiances in ensemble kalman filters. *Mon. Wea. Rev.*, **138**, 282–290.

451 Du, J. and C. Ma, 2013: Vector random fields with compactly supported covariance matrix  
 452 functions. *J. Stat. Plan. Infer.*, **143**, 457–467.

453 Gaspari, G. and S. E. Cohn, 1999: Construction of correlation functions in two and three dimensions. *Q. J. R. Meteorol. Soc.*, **125**, 723–757.

454

455 Genton, M. G. and W. Kleiber, 2015: Cross-covariance functions for multivariate geostatistics  
456 (with discussion). *Statist. Sci.*, **30**, 147–163.

457 Hamill, T. M., J. S. Whitaker, and C. Snyder, 2001: Distance-dependent filtering of background  
458 error covariance estimates in an ensemble Kalman filter. *Mon. Wea. Rev.*, **129**, 2776–2790.

459 Houtekamer, P. L. and H. L. Mitchell, 1998: Data assimilation using an ensemble Kalman filter  
460 technique. *Mon. Wea. Rev.*, **126**, 796–811.

461 Houtekamer, P. L. and H. L. Mitchell, 2001: A sequential ensemble Kalman filter for atmospheric  
462 data assimilation. *Mon. Wea. Rev.*, **129**, 123–137.

463 Hunt, B. R., E. J. Kostelich, and I. Szunyogh, 2007: Efficient data assimilation for spatiotemporal  
464 chaos: A local ensemble transform Kalman filter. *Physica D*, **230**, 112–126.

465 Jun, M., I. Szunyogh, M. G. Genton, F. Zhang, and C. H. Bishop, 2011: A statistical investigation  
466 of the sensitivity of ensemble-based Kalman filters to covariance filtering. *Mon. Wea. Rev.*, **139**,  
467 3036–3051.

468 Kang, J.-S., E. Kalnay, J. Liu, I. Fung, T. Miyoshi, and K. Ide, 2011: “Variable localization”  
469 in an ensemble Kalman filter: Application to the carbon cycle data assimilation. *J. Geophys.  
470 Res.*, **116**, doi:10.1029/2010JD014673.

471 Kleiber, W. and E. Porcu, 2015: Nonstationary matrix covariances: Compact support, long  
472 range dependence and adapted spectra. *Stoch. Environ. Res. Risk Assess.*, **29**, 193–204.

473 Lei, L. and J. Anderson, 2014: Comparison of empirical localization techniques for serial ensemble  
474 kalman filters in a simple atmospheric general circulation model. *Mon. Wea. Rev.*, **141**, 4140–  
475 4153.

476 Lorenz, E. N., 1995: Predictability-A problem partly solved. Proceedings of the Seminar on  
477 Predictability, vol. 1. ECMWF, Reading, Berkshire, UK.

478 Lorenz, E. N., 2005: Designing chaotic models. *J. Atmos. Sci.*, **62**, 1574–1587.

479 Ott, E., et al., 2004: A local ensemble Kalman filter for atmospheric data assimilation. *Tellus*,  
480 **56A**, 415–428.

481 Porcu, E., D. J. Daley, M. Buhmann, and M. Bevilacqua, 2012: Radial basis functions with  
482 compact support for multivariate geostatistics. *Stoch. Environ. Res. Risk Assess.*, **27**, 909–  
483 922.

484 Whitaker, J. S. and T. M. Hamill, 2002: Ensemble data assimilation without perturbed obser-  
485 vations. *Mon. Wea. Rev.*, **130**, 1913–1924.

486 Wilks, D. S., 2006: *Statistical methods in the atmospheric sciences*. Academic Press, Amsterdam.

487 Zhang, H. and J. Du, 2008: Covariance tapering in spatial statistics. Positive Definite Functions:  
488 From Schoenberg to Space-Time Challenges, eds. J. Mateu and E. Porcu, Gráficas Castañ,  
489 Spain.

490 **List of Figures**

491 1	The Gaspari-Cohn covariance function with a localization constant $c = 25$ (sup-	27
492 port of 50) and the Askey covariance function $f(d; \nu, c) = (1 - \frac{d}{c})_+^\nu$ , with a support		
493 parameter $c = 50$ and various shape parameters.		
494 2	A snapshot of the variables $X$ and $Y$ from a numerical integration of the system	28
495 of Eqs. (14) and (15) with $K = 36$ , $J = 10$ , $F = 10$ , $a = 10$ , $b = 10$ , and $h = 2$ .		
496 3	Spatial locations of partial observation of $X$ and $Y$ .	29
497 4	The probability distribution of RMSE for variable $X$ in the case when the system is	
498 only partially observed. Results are shown for different localization strategies. For		
499 the definitions of localization strategies S1, S2, S3 and S4, see the text. The title		
500 of each panel indicates the localization radius (length of support). The numbers		
501 below S4 indicate the value of $\beta$ .		30
502 5	Same as 4, except for variable $Y$ .	31
503 6	Same as 4, except for the case when the system is fully observed.	32
504 7	Same as 6, except for variable $Y$ .	33
505 8	Same as 4, except for 500 ensemble members.	34
506 9	Same as 5, except for 500 ensemble members.	35
507 10	Same as 6, except for 500 ensemble members.	36
508 11	Same as 7, except for 500 ensemble members.	37

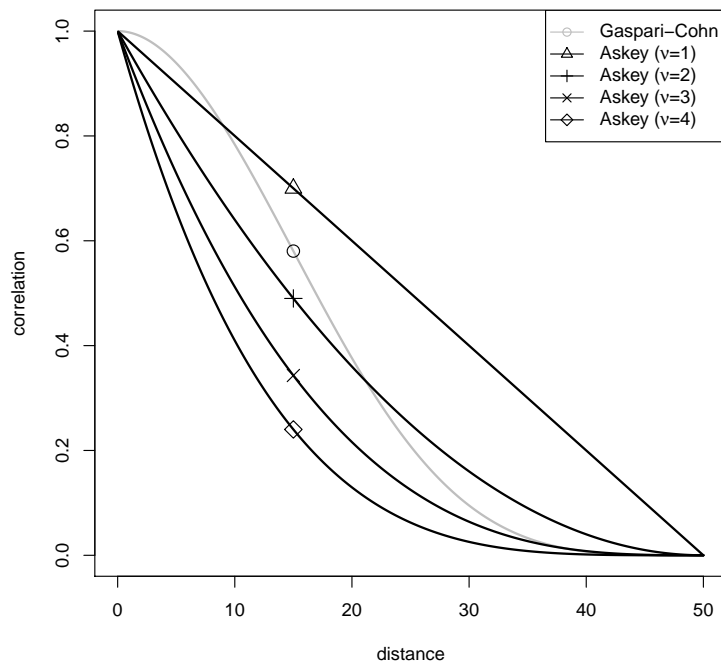


Figure 1: The Gaspari-Cohn covariance function with a localization constant  $c = 25$  (support of 50) and the Askey covariance function  $f(d; \nu, c) = (1 - \frac{d}{c})_+^\nu$ , with a support parameter  $c = 50$  and various shape parameters.

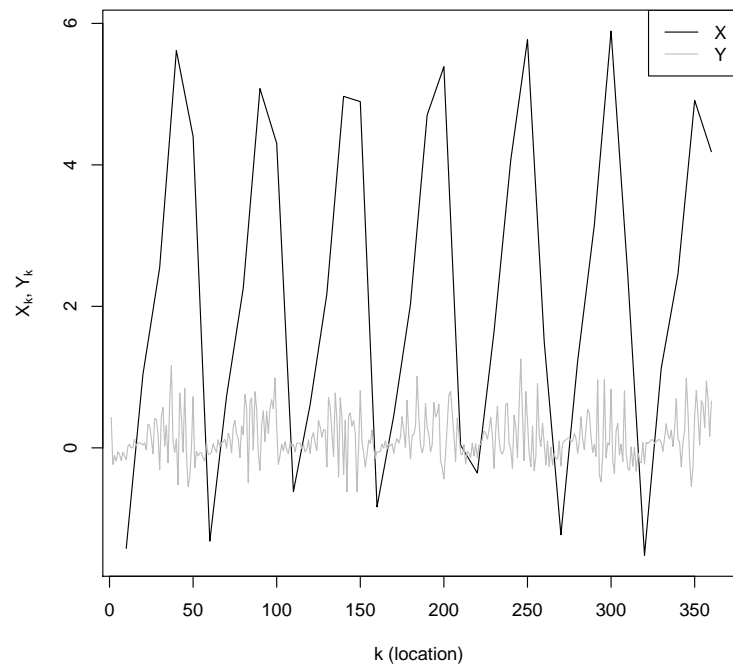


Figure 2: A snapshot of the variables  $X$  and  $Y$  from a numerical integration of the system of Eqs. (14) and (15) with  $K = 36$ ,  $J = 10$ ,  $F = 10$ ,  $a = 10$ ,  $b = 10$ , and  $h = 2$ .

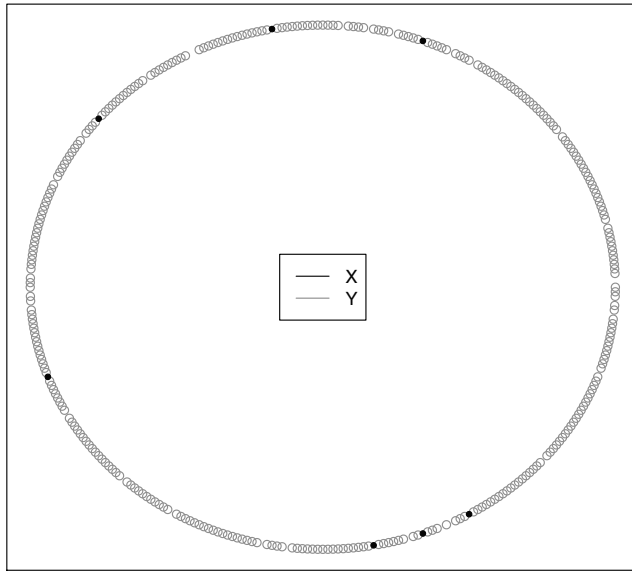


Figure 3: Spatial locations of partial observation of  $X$  and  $Y$ .

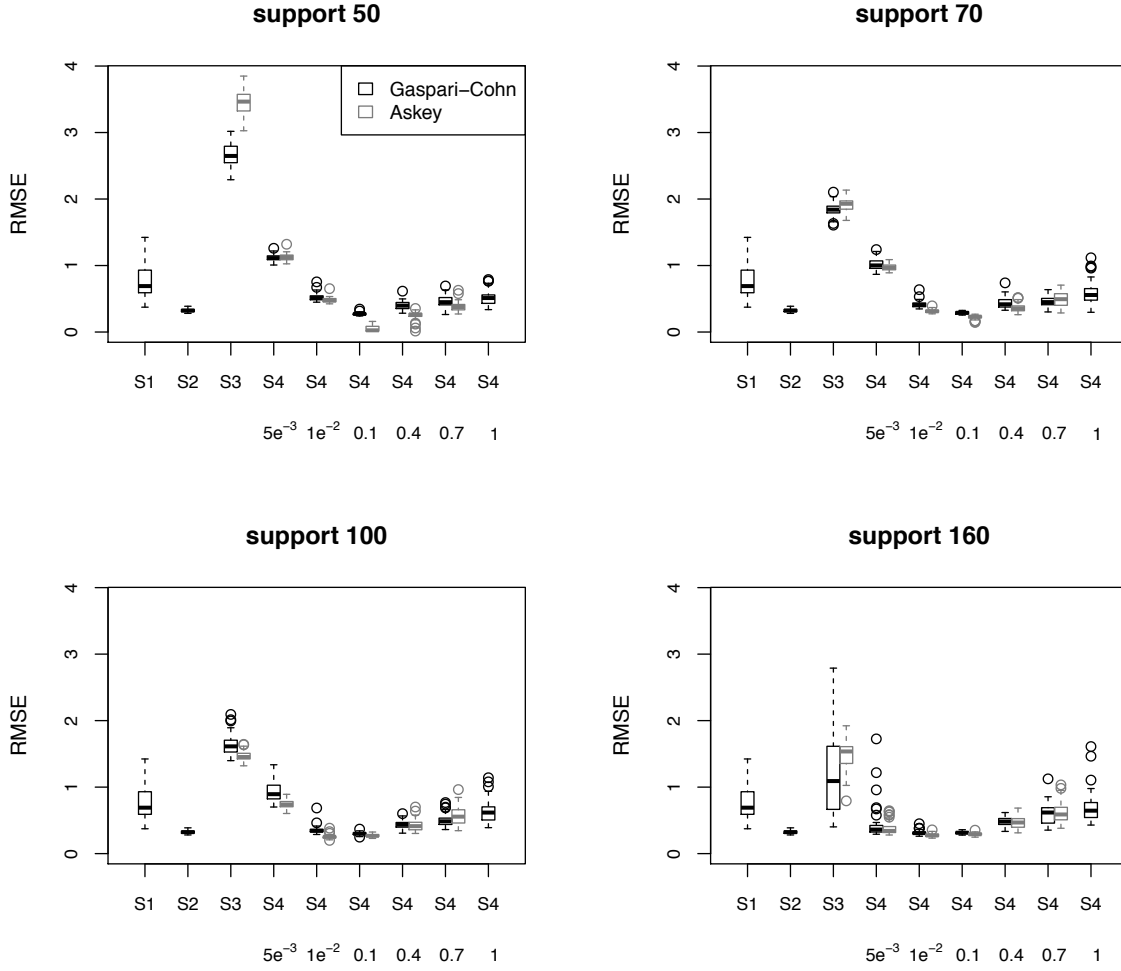


Figure 4: The probability distribution of RMSE for variable  $X$  in the case when the system is only partially observed. Results are shown for different localization strategies. For the definitions of localization strategies S1, S2, S3 and S4, see the text. The title of each panel indicates the localization radius (length of support). The numbers below S4 indicate the value of  $\beta$ .

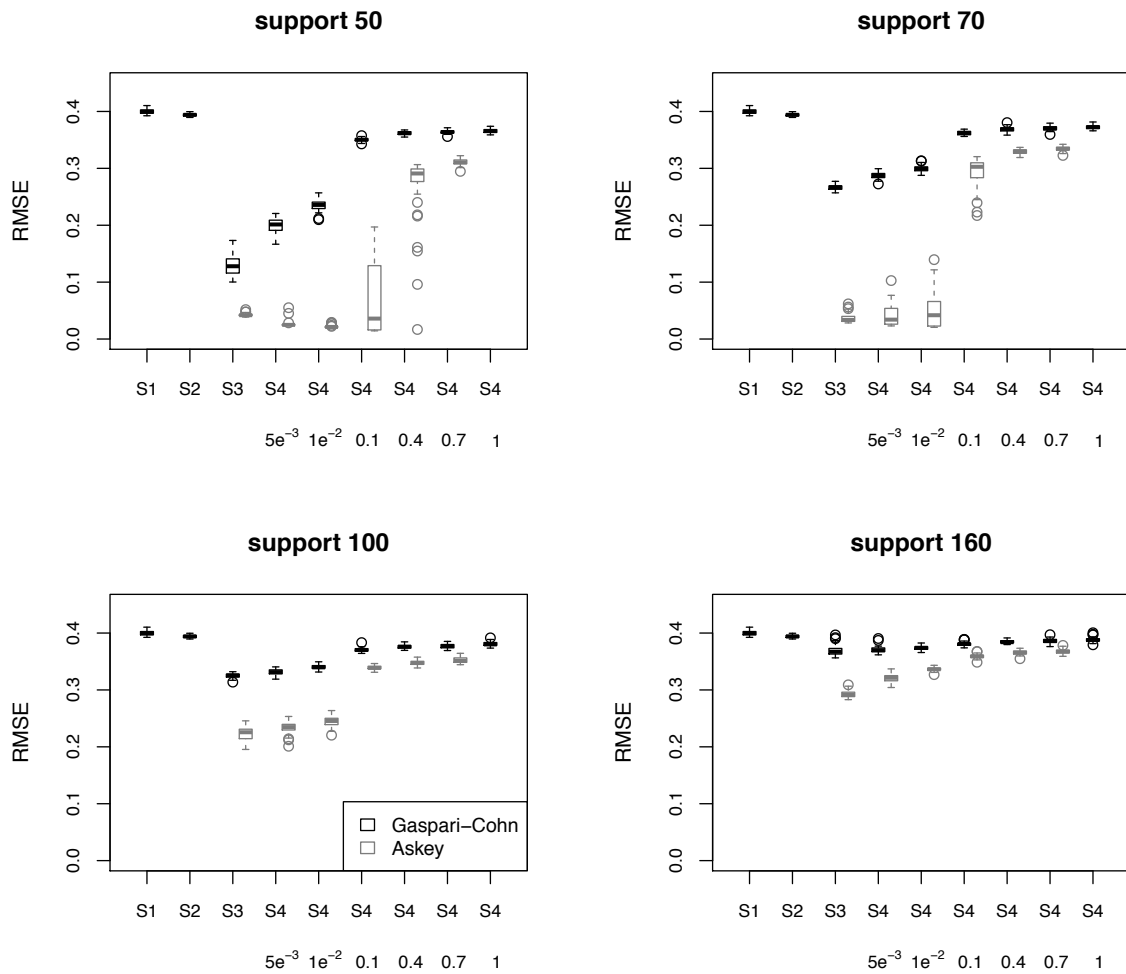


Figure 5: Same as 4, except for variable  $Y$ .

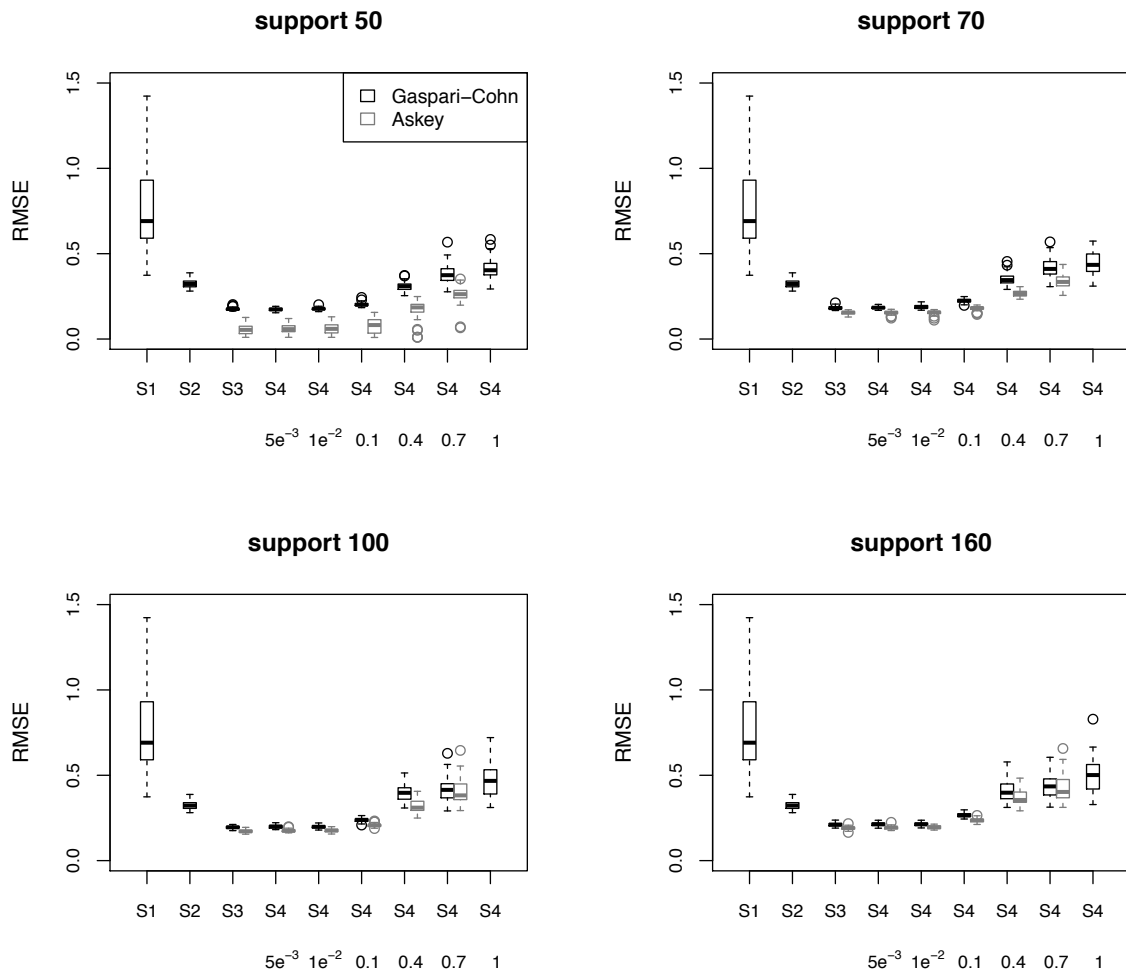


Figure 6: Same as 4, except for the case when the system is fully observed.

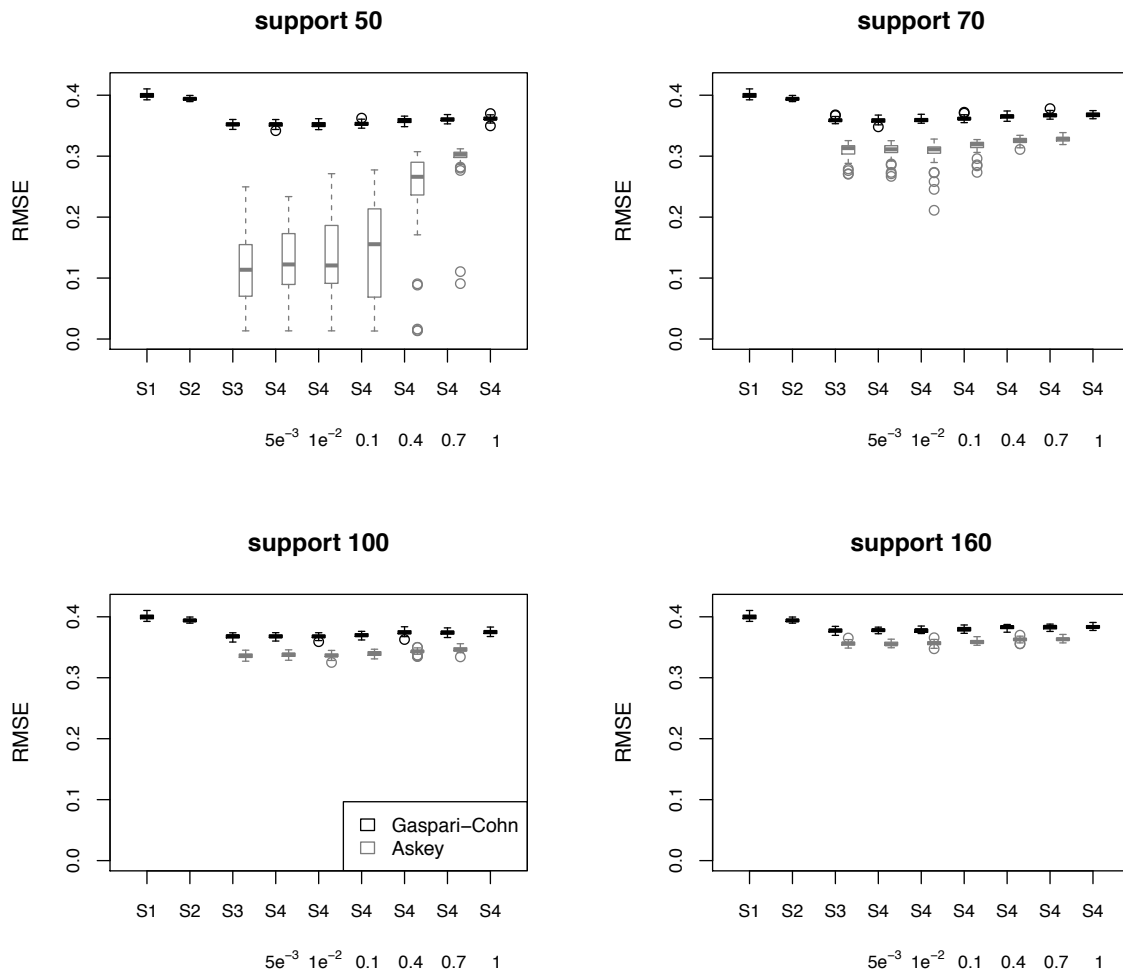


Figure 7: Same as 6, except for variable  $Y$ .

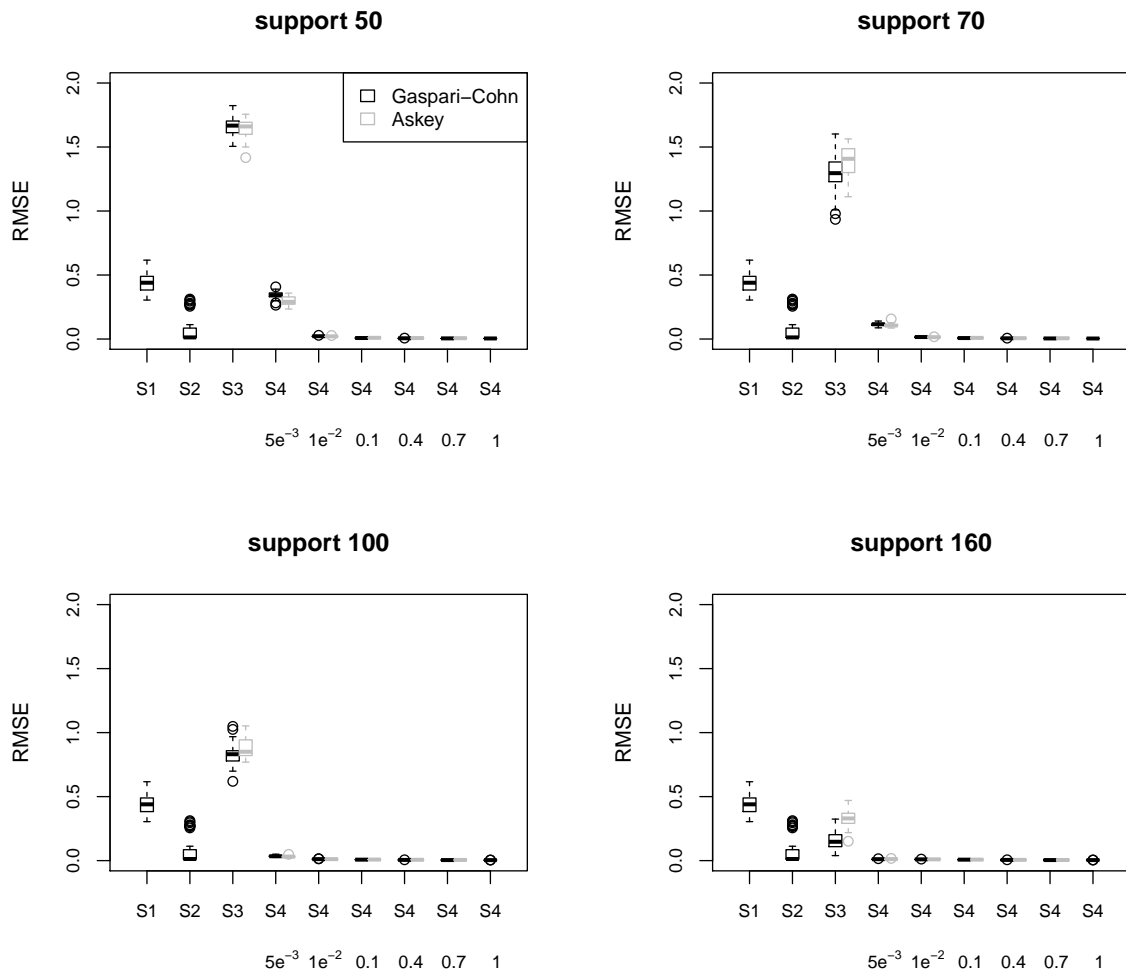


Figure 8: Same as 4, except for 500 ensemble members.

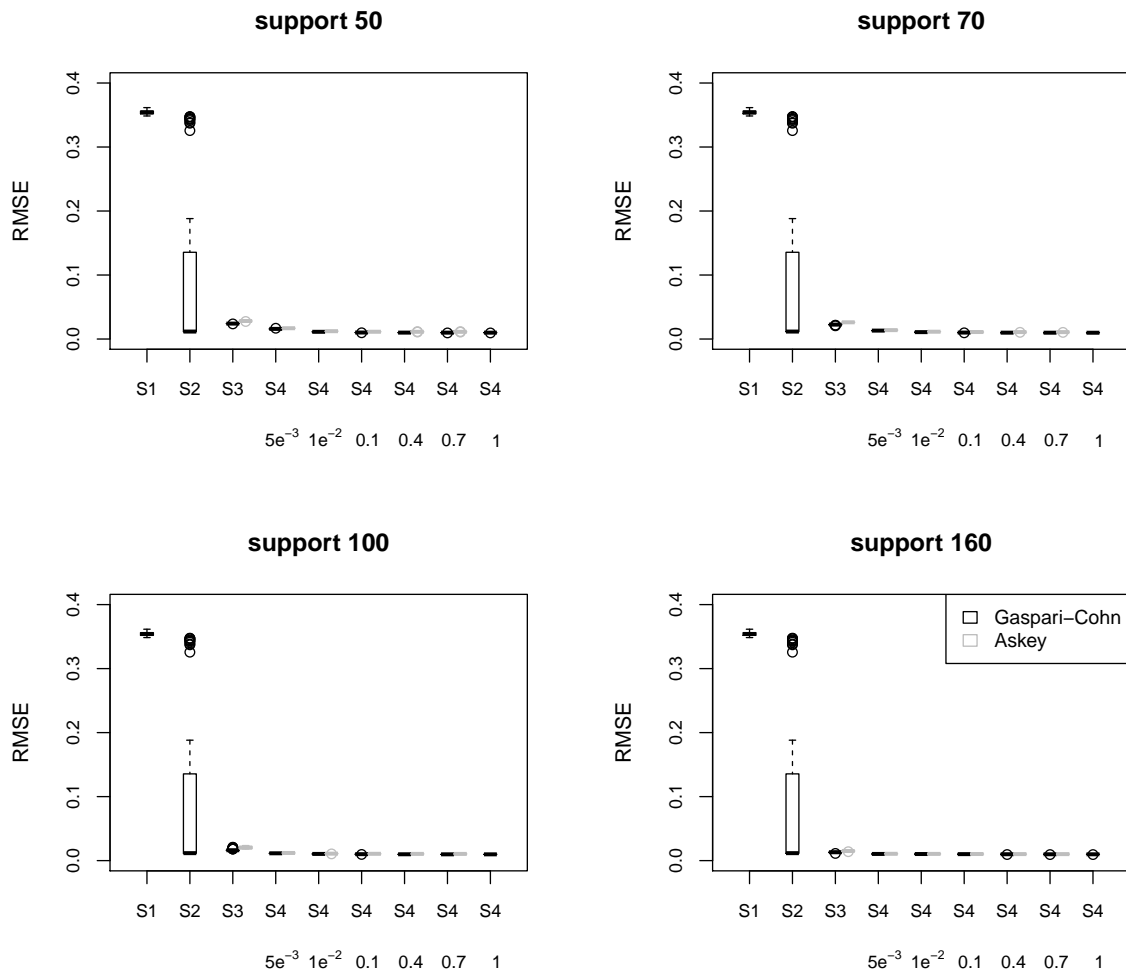


Figure 9: Same as 5, except for 500 ensemble members.

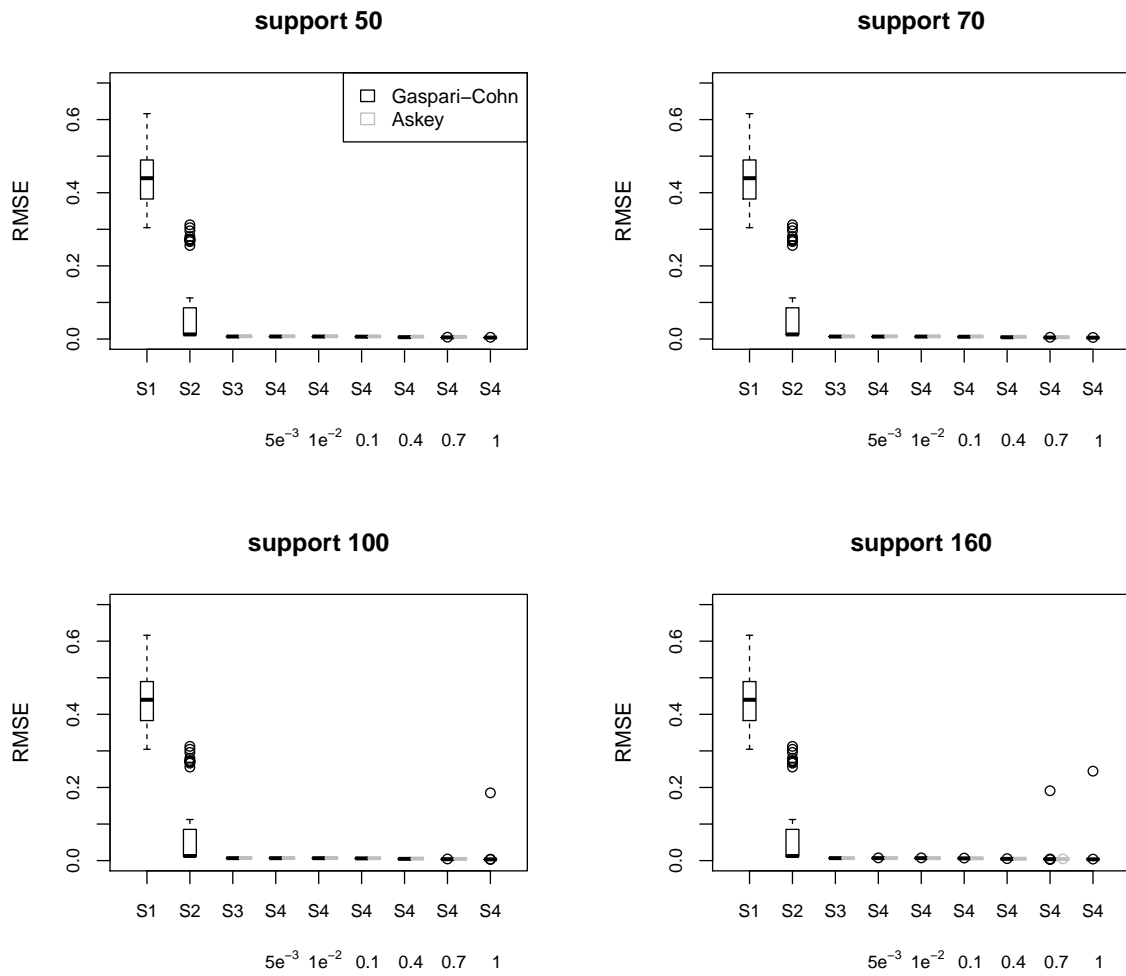


Figure 10: Same as 6, except for 500 ensemble members.

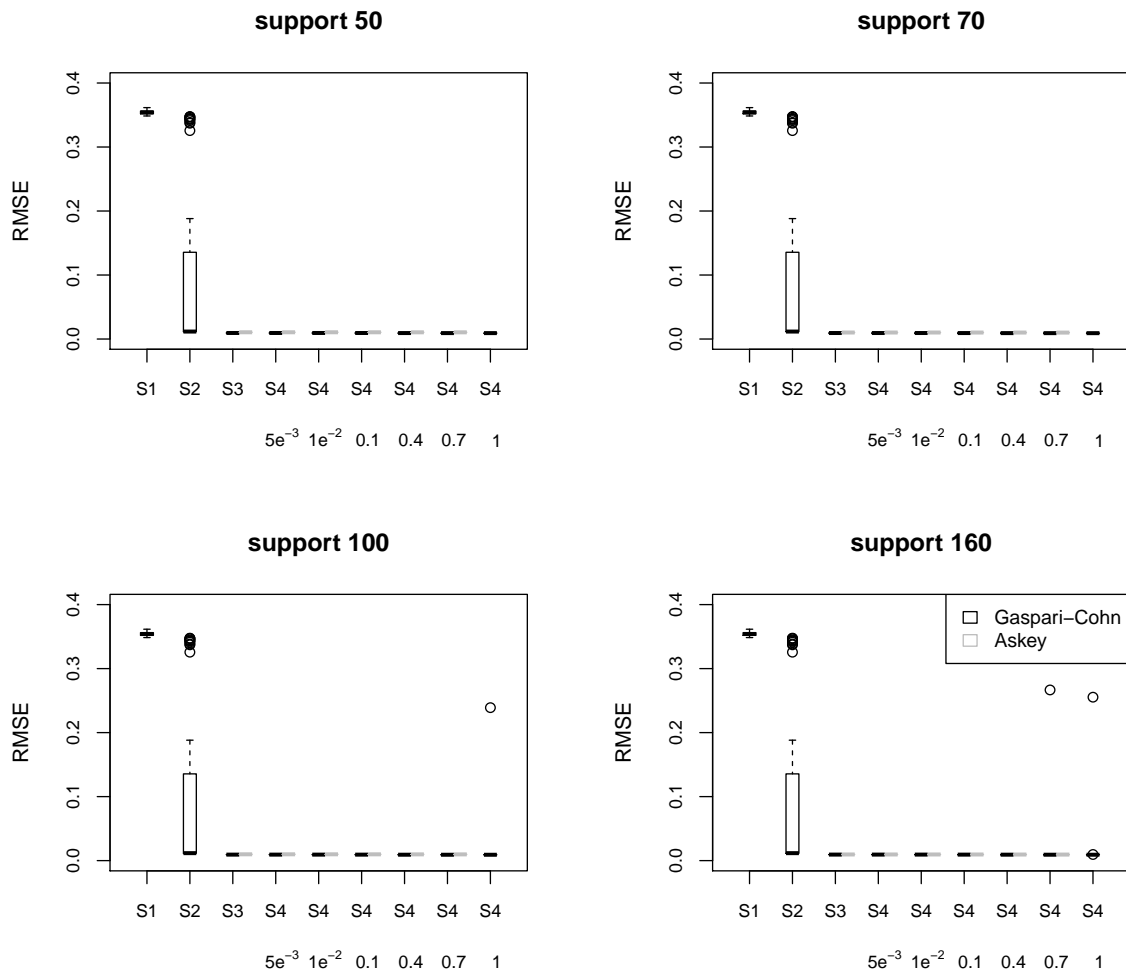


Figure 11: Same as 7, except for 500 ensemble members.